Study of the crystalline phase orientation in uniaxially stretched polypropylene by Raman spectroscopy: Validation and use of a time-resolved measurement method

Julien Martin, Marc Ponçot, Patrice Bourson, Abdesselam Dahoun, Jean-Marie Hiver

▶ **To cite this version:**

Julien Martin, Marc Ponçot, Patrice Bourson, Abdesselam Dahoun, Jean-Marie Hiver. Study of the crystalline phase orientation in uniaxially stretched polypropylene by Raman spectroscopy: Validation and use of a time-resolved measurement method. Polymer Engineering and Science, 2011, 51 (8), pp.1607-1616. ⟨10.1002/pen.21944⟩. ⟨hal-03612294⟩

HAL Id: hal-03612294

https://hal.univ-lorraine.fr/hal-03612294v1

Submitted on 31 Jan 2023

HAL is a multi-disciplinary open access archive for the deposit and dissemination of scientific research documents, whether they are published or not. The documents may come from teaching and research institutions in France or abroad, or from public or private research centers.

L'archive ouverte pluridisciplinaire **HAL**, est destinée au dépôt et à la diffusion de documents scientifiques de niveau recherche, publiés ou non, émanant des établissements d'enseignement et de recherche français ou étrangers, des laboratoires publics ou privés.

HAL Authorization

Study of the crystalline phase orientation in uniaxially stretched polypropylene by Raman spectroscopy: validation and use of a time-resolved measurement method

J. Martin[(1,2)*], M. Ponçot[(2,3)], P. Bourson[(1)], A. Dahoun[(2)], J.M. Hiver[(2)]

(1) Laboratoire Matériaux Optiques, Photonique et Systèmes, Université de Metz et Supélec, UMR CNRS 7132, 2 rue Edouard Belin, 57070 Metz, France

(2) Institut Jean Lamour, département Science et Ingénierie des Matériaux et de la Métallurgie, UMR CNRS 7198, Nancy Université, Parc de Saurupt, 54042 Nancy, France

(3) ArcelorMittal R&D Automotive Applications Montataire, BP 30109, 1 route de Saint Leu, 60761 Montataire Cedex

** Author to whom correspondence should be addressed*

ABSTRACT

A method based on the intensity sensitivity of two Raman scattering bands (973 and 998 cm^{-1}) to laser light polarization is proposed to quantify the molecular orientation of the crystalline phase in isotactic polypropylene. This paper is firstly devoted to the validation of the method by comparing Raman and Wide Angle X-ray Scattering (WAXS) measurements performed on *post mortem* test samples uniaxially deformed at growing levels. The method is secondly applied to follow the molecular orientation in real-time during the course of a tensile test. *Post mortem* results show a quantitative agreement between Raman and WAXS measurements. *In situ* results mainly evidence the ability of the Raman method to characterize molecular orientation in real-time with less than 5 second time resolution. Comparison between *post mortem* and *in situ* results gives insight of relaxation mechanisms occurring in material after unloading.

KEYWORDS

Isotactic Polypropylene; Uniaxial Tension; Deformation Mechanisms; Molecular Orientation; Relaxation; Wide Angle X-ray Scattering (WAXS); Raman Spectroscopy; Real-time measurements

INTRODUCTION

To gain a better understanding of the macroscopic mechanical properties of materials, especially for solid polymers, it is fundamental to understand the mechanisms of deformation which take place at the microstructure scale [1]. In the specific case of semi-crystalline polymers which exhibit a complex morphology mixing a disordered amorphous and an ordered crystalline phase, mechanical properties are mainly dependent on both the degree of crystallinity and the macromolecular orientation [1-3]. At the macroscopic scale, mechanical properties of such materials are usually determined using conventional uniaxial tensile tests [5]. At the microscopic scale, a number of analytical techniques can be used to investigate the microstructure such as thermal analysis, microscopic observations, X-ray diffraction, birefringence, nuclear magnetic resonance and vibrational spectroscopic techniques [6, 7]. By collecting both these macroscopic and microscopic data, numerous experimental works have attempted to associate one state of deformation (such as the strain level) to one state of microstructure (such as molecular orientation) in order to propose elementary descriptive models of the deformation micro-mechanisms [8-10]. However, in many cases, evidence of these mechanisms is debatable for two major experimental limits:

i) In the case of ductile materials which experience a pronounced necking due to their plastic instability (such as polymers), conventional mechanical tests giving access to the engineering stress – strain curve are inappropriate to reveal their intrinsic mechanical behaviour at prescribed temperature and strain rate.

ii) Moreover, usual analytical techniques require in most of the cases *post mortem* analyses and destructive sampling procedures coupled with serious risk of uncontrolled relaxational changes. In a recent paper, Tanaka and Young [] point out advantages and disadvantages of several techniques such as wide angle X-ray scattering WAXS, birefringence measurements, nuclear magnetic resonance and vibrational techniques for the

characterization of the molecular orientation in polymers. Birefringence can be employed for rapid measurements but the orientation information is averaged over the crystalline and amorphous region. In the case of highly crystalline polymers, the measurement is also likely to be influenced by sample opacity. WAXS is a useful method for the study of crystallite orientation with accuracy. Using synchrotron radiations, this technique allows performing time-resolved measurements with less than 100 ms time resolution. Nevertheless access to beamline is often too restrictive for ordinary measurements. Focusing on the vibrational spectroscopic approaches, both infrared (IR) dichroism measurement and polarized Raman spectroscopy was found to be powerful techniques for quantitative and in real-time measurement of molecular orientation distribution both in amorphous and crystalline phase. However, the major limitation of IR method is that samples have to be highly transparent and thin for the absorbance measurement.

In this work we propose to overcome these two experimental difficulties by combining both a tensile system which provides the true mechanical behaviour of a material and a polarized Raman micro-spectrometer. This systeme is used to characterize the molecular orientation in crystalline phase of isotactic polypropylene. The study is divided into two parts. The first one deals with the validation of a specific measurement method based on the intensity sensitivity of two specific polarized Raman bands (at 973 and 998 cm^{-1}) to orientation of crystalline chains. Method has been qualitatively used in a previous paper to discriminate orientation of lamellae within one β-iPP spherulite. Its reliability is examined by comparing Raman results with the well-established Hermans' orientation function calculated from WAXS measurements performed on the same post mortem stretched samples. The second part of the study is attached to demonstrate the ability of the method to measure orientation *in situ* with the deformation (5 s time resolution) over a large true strain range, from the elastic to the hardening stage of iPP.

EXPERIMENTAL DETAILS

Material

The investigated polypropylene was manufactured by Atochem under the reference 3050 MN1. Molecular weight distribution of this isotactic grade was investigated by gel permeation chromatography. Polypropylene was dissolved in trichlorobenzene at 150 °C in order to obtain a 2 $g.l^{-1}$ concentrated solution. Solution was then stabilized with ionol. Analyses were performed at 145 °C. IPP is characterized by a relatively broad molecular weight distribution with $\overline{M}_w$ = 262000 $g.mol^{-1}$ and $\overline{M}_n$ = 75900 $g.mol^{-1}$. Pellets of polymer were processed by injection-moulding into rectangular plates (200×200×4 mm) as shown in figure 1. The process consists of filling the mould maintained at 30 °C with the polymer melt at 240 °C, under a pressure of 1200 bars. The cooling sequence is about 240 s. As it is well reported in literature, injection-moulding process induces the development of an oriented superficial layer, usually termed as a skin layer [ ]. It is the result of a shear stress at the wall of the cooled mould. Pictures of the figure 2, recorded with a polarized light optical microscope on a thin cross-sectional slice (20 µm thickness) extracted from the center of a plate evidences an anisotropic superficial layer of about 360 µm thickness. The core region is isotropic with an important amount of α-spherulites of about 55 µm average diameter. In order to prevent measurement interferences with the molecular orientation induced by the deformation, skin layers of each specimen are previously eliminated by polishing flat surfaces. Polishing procedure is maintained identical for each specimen. Moreover to insure reproducibility, specimens are always extracted from the same location in the plate namely in its center far-away from the injection gate and the walls of the mould (figure 1). Material density in the core region is determined by hydrostatic weighting, ρ = 0.908 $g.cm^{-3}$. Based on values published in the literature for perfectly crystalline and amorphous phase (ρ_c = 0.946

$g.cm^{-3}$ and ρ_a = 0.854 $g.cm^{-3}$, respectively [24]), the weight degree of crystallinity is found to be equal to 59 %. This value is confirmed by differential scanning calorimetry measurements performed at a heating rate of 10 °C.min^{-1}. Thermograms show a melting point located at 165 °C with an enthalpy of fusion equal to 96 $J.g^{-1}$. This corresponds to a weight degree of crystallinity of about 58 % (the enthalpy of fusion considered for a perfect crystal of infinite size is 165 $J.g^{-1}$ [24]). X-ray scattering measurement performed in the core region with a Cu-$K_{\alpha 1}$ radiation (λ = 0.1542 nm) proves the semi-crystalline nature of the investigated iPP. Narrow peaks observed at 2θ = 14.1, 16.9, 18.5, 21.2 and 21.8 degrees show the presence of α-iPP crystals in majority. They are due to the selective diffraction of the (110), (040), (130), (111) and ($\bar{1}$31) crystallographic planes of the α-iPP monoclinic unit cell respectively [25]. The broad halo noted at $2\theta \approx$ 16.5 degrees is attributed to the X-ray diffusion of the amorphous phase.

Test specimens are machined out from the injection-molded plates into dumbbell-shape specimens with overall dimensions of 90 x 10 x 4 mm^3 (Figure 1). As recommended in previous works using the VideoTraction^{TM} system, the median region is reduced to 9 mm in order to localize necking in this predefined zone, the Representative Volume Element (RVE) [26, 27]. Massive heads on both sides are designed to be gripped in jaws of the tensile machine.

Post mortem measurements

The main objective of *post mortem* measurements is to define the Raman measurement method and validate its use. For this purpose, specimens are stretched and unloaded at various strain level inducing different degree of the molecular orientation. Last one is firstly determined by WAXS measurements and then compared to Raman results.

The video-controlled mechanical testing method used here is the VideoTraction™ which was developed by G'Sell and Hiver [29]. Figure 3 is a schematic view of the system. It gives access to the constitutive plastic behaviour of polymers under uniaxial tension by measuring in real time the true strain ε_{zz} (even after the necking phenomenon has appeared) and the true stress σ_{zz} in a given local material element (Representative Volume Element RVE or necking zone) while its local true strain rate is maintained at a constant value during the test. Technical explanations of the method principle were widely presented elsewhere before [14, 15]. In our study, all tests are carried out at 30 °C under a monotonous strain rate maintained at $\dot{\varepsilon}_{zz} = 5.10^{-3}$ s^{-1}. Various specific true strain values are chosen. They are summarized in table 1. Under load they are: ε_{zz} = 0.06, 0.15, 0.3, 0.5, 0.8, 1 and 1.2. The non-deformed sample, ε_{zz} = 0, is taken into account in this study as the material microstructure reference. For each test, the sample is unloaded and the evolution of the axial true strain is followed during 3 hours. Addiego et al. [27], Martin [31] and Ponçot [32] show that after 3 h of recovery at zero stress, the axial true strain keeps nearly stable. The residual true strain, $\varepsilon_{zz,r}$, is recorded at the end of this period.

Non-deformed and recovered samples are analysed by WAXS, using the Debye-Scherrer method [2, 3]. In the case of uniaxial deformation, many authors have identified a "fibre texture" oriented towards the z-tensile direction (cylindrical symmetry) [35-37]. This presupposes that analysis of one 2D-WAXS pattern is sufficient to describe the 3D-spatial arrangement of the crystallites within the polymer. Before WAXS analysis, thickness of samples is reduced to 1 mm by polishing. The analyzed zone is the RVE. Diffraction system and experimental conditions used here are described in details by Addiego et al. [Addiego]. On each pattern, an absorption correction is brought to the intensity magnitude, I, by the Lambert's law, $I = I_0\exp(-\mu t/\cos(2\theta))$, where 2θ is the diffraction angle, μ the absorption coefficient equal in this case to 3.85 cm^{-1} and t = 1 mm the sample thickness [27, 32].

Average orientation of iPP crystallites is quantified by the Hermans'orientation functions, $f_{x/z}$, which describes the orientation of a given crystallographic axis **x** relative to one reference direction, usually the **z**-axis stretching direction [23]. In this paper, we have considered the specific orientation function $f_{c/z}$ since **c**-axis of the α-iPP unit cell is also parallel to the helical axis of the macromolecular chains. Since no (00l) pure **c**-axis reflections are present in the α-iPP WAXS pattern, $f_{c/z}$ is calculated by the combination of two reflecting crystal planes e.g., the (040) and (110) planes [Wilchinsly et dahoun].

$$\langle \cos^2\rho_{c/z}\rangle = 1 - \frac{(b^2+a^2\sin^2\beta)\langle \cos^2\rho_{110/z}\rangle - (a^2\sin^2\beta-b^2)\langle \cos^2\rho_{040/z}\rangle}{b^2} \qquad (1)$$

The terms a = 0.665 nm and b = 2.096 nm are two of the three α-iPP unit cell parameters and β = 99 degrees, the angle formed between **a** and **c**-axis [40]. The function $f_{c/z}$ varies from a value +1 for **c**-axis oriented parallel to the **z** stretching direction, through a value 0 for randomly oriented crystals, to a value -0.5 for **c**-axis oriented perpendicular to the **z**-stretching direction.

Raman scattering experiments are performed on non-deformed and *post mortem* deformed samples using an Aramis® microspectrometer (Horiba Jobin Yvon, Lille, France). A diode laser emitting a 785 nm exciting line is used and allows a substantial reduction in fluorescence. When the laser beam is focused onto the sample, the illumination power density measured on the sample is kept between 15 and 20 $mW.\mu m^{-2}$. All spectra are recorded in backscattered geometry using a 1200 $grooves.mm^{-1}$ as the diffraction grating and a spectral resolution of about 0.6 cm^{-1} is achieved. Previously, the Raman shift was calibrated with the strong peak at 521 cm^{-1} of silicon. Both the incident and scattered lights are collected through an Olympus confocal microscope (100× objective lens, 1000× total magnification, Numerical Aperture NA = 0.9). Rayleigh scattered light is blocked by using a holographic Notch filter. A

half-wave plate is installed on the apparatus allowing the polarization direction of the incident laser radiation to be control. A polarizer is also placed on the backscattering optical path to polarize the Raman scattering radiation. Acquisition time is equal to 20 s and final spectrum is an average of ten spectra. A self-written fitting least-square procedure based on the Levenberg-Marquardt method is used to process spectral data [33]. Residual fluorescence background is eliminated by a polynomial baseline cutting procedure. A mixed Gaussian-Lorentz function is used to decompose each scattering band. Final adjustment gives access to the useful features as position, integrated intensity and full width at half maximum [34].

In situ measurements

The main objective of *in situ* measurements is to apply the Raman measurement method during the entire course of a tensile test. For this purpose a system coupling a Raman spectrometer and the VidéoTraction™ system is featured (figure 3). Specimens are also machined out from the injection-moulded plates as indicated in figure 1. Contrary to *post mortem* experiments, thickness of samples is considerably reduced to 500 µm (by polishing). Main reason is to minimize the deflection of the necking zone ensuring a suitable focalisation of the Raman laser onto the sample during the tensile test. On the same occasion, oriented superficial layers induced by the processing conditions are eliminated.

Raman spectra are collected in backscattered geometry using an iHR250® microspectrometer (Horiba Jobin Yvon, Lille, France) linked to a remote head of probe by means of two optic fibres. The head of probe, placed in face to face to the video-controlled system is equipped with an Olympus long working distance objective lens (12 mm focal). Laser radiation coming from a diode laser (λ = 785 nm) is maintained focused onto the predefined RVE zone where necking appears. A linear polarizer and analyser are also installed in the head of probe. They allow polarizing the incident laser beam and the Raman scattering respectively. Rayleigh scattered light is eliminated through a holographic Notch

filter placed on the light path before the diffraction grating, 1200 grooves.mm^{-1}. The spectral resolution achieved is about 0.6 cm^{-1}. Conditions of spectral treatment are quite identical as *post mortem* measurements.

The sample is deformed at 30 °C until its rupture at ε_{zz} = 1.6 under a constant true strain rate, $\dot{\varepsilon}_{zz}$ = 5.10^{-3} s^{-1}. Contrary to *post mortem* analyses, acquisition time is considerably reduced to 5 s. Mean reason is to minimize structural changes which take place during this period of time. It allows recording 40 spectra during the tensile test. Thus one spectrum corresponds to a strain variation $\Delta\varepsilon_{zz}$ of about 0.04. The experiment is repeated 5 times in the same conditions to ensure reproducibility.

RESULTS AND DISCUSSION

Mechanical behaviour

Figure 4 (a) shows the evolution of the true axial stress – strain curve ($\sigma_{zz} - \varepsilon_{zz}$) of the iPP under uniaxial tension at 30 °C remaining a constant axial true strain rate $\dot{\varepsilon}_{zz}$ = 5.10^{-3} s^{-1}.The stress – strain curve, typical of semi-crystalline polymers, is characterized by three different regimes: i) In the elasto-viscoelastic regime, ε_{zz} = 0 - 0.09, the initial slope of the curve is related to the elastic Young's modulus, noted E (E = 1.7 GPa). The yield point is defined when stress σ^{y}_{zz} achieves 36 MPa and passes through a round-off maximum at strain ε^{y}_{zz} = 0.09. ii) In the plastic regime, ε_{zz} = 0.09 – 0.8, stress is firstly marked by a small stress decrease while the deformation localizes in a sharp neck in the RVE. This is then followed by a symmetric propagation of the neck shoulders towards the specimen heads. iii) In the plastic stress-hardening regime, ε_{zz} = 0.8 – 1.6, stress increases exponentially from 32 to 75 MPa.

An example of the axial strain evolution during unloading and recovery is presented in figure 4 (b). In this case, the specimen is deformed until the applied strain reaches 0.8 (step

denoted 0 to 1), subsequently unloaded at a strain rate opposite to the initial loading strain rate (step 1 to 2) and finally left to recover at zero stress for 3 h (step 2 to 3). The axial strain drops from 0.8 to 0.71 during the unloading period and from 0.71 to 0.52 during the recovery. Thus the residual axial strain is $\varepsilon_{zz,r} = 0.52$. Table 1 summarized the residual axial strains recorded for each *post mortem* deformed sample under consideration.

Post mortem results

Figures 5 (a)-(d) show the WAXS patterns obtained on deformed samples ($\varepsilon_{zz,r} = 0$, 0.15, 0.52 and 0.79). Pattern of the non-deformed sample evidences a set of homogeneous scattering rings characteristics of an isotropic spatial distribution of crystallites within the polymer [2, 3]. Shape of patterns varies with the increasing deformation since rings get shorter. For the maximum residual true strain achieved, $\varepsilon_{zz,r} = 0.79$, the pattern shows sharp spots typical of an anisotropic spatial distribution of crystallites. The Hermans' orientation function $f_{c/z}$ is calculated and plotted versus the residual true strain in figure 7 (a). Error bars are statistically determined from measurements performed on five stretched samples and is quite identical for all samples. The orientation function $f_{c/z}$ of the non-deformed sample is found to be equal to 0.04. It is closed to the value of a perfectly isotropic oriented material. Nevertheless this indicates that a subtle residual crystalline orientation induced by the injection-moulding process can't be excluded [28]. Globally the increase of the orientation function $f_{c/z}$ with respect to the residual true strain is consistent with a gradual alignment of the **c**-crystallographic axis towards the **z**-stretching direction.

Figures 6 (a) shows whole spectra recorded on a non-deformed ($\varepsilon_{zz,r} = 0$) and a large deformed ($\varepsilon_{zz,r} = 0.79$) samples by using an **x(zz)x** polarization configuration according to Porto's nomenclature [41]. In this configuration, electric fields of both incident and scattered lights are parallel to the **z**-stretching direction. Raman scattering is thus excited and collected principally from chemical bonds oriented towards the z-direction. Figure 6 (b) shows

influence of the deformation on the intensity of two Raman bands at 973 and 998 cm^{-1}(after spectral adjustement). They are attributed exclusively to macromolecules in the 3_1 helical conformation of the iPP crystalline phase [13-15]. The first one is assigned principally to the C-C asymmetric stretching mode of the skeletal backbones while the second is referred to the rocking mode of the CH_3 alkyl groups in lateral position on the chain. Intensity of the 973 cm^{-1} band is high for the deformed sample since proportion of C-C bonds oriented towards the z-tensile direction is high. Situation is just opposite for the 998 cm^{-1} since CH_3 alkyl groups are less numerous being oriented in the z-tensile direction. On the basis of this observation, we propose the use of the intensity bands ratio I_{973} / I_{998} to estimate orientation of the iPP crystalline chains. Method is applied on deformed samples. Figure 7 (a) shows evolution of the bands ratio I_{973} / I_{998} versus the residual true strain ε_{zz}. Error bars correspond to the standard deviation calculated from ten spectra recorded on the RVE of five stretched samples. As expected the Raman bands ratio increases with the increasing deformation. It reflects a progressive orientation of the C-C skeletal backbones of the crystalline chains towards the **z**-tensile direction. Its evolution is comparable with the Herman's orientation function, $f_{c/z}$. Figure 7 (b) attests of a good agreement between the two series of data since a linear correlation is obtained. Correlation coefficient is closed to 1. In the strain range considered, the linear correlation ensures the reliability of the Raman measurement method. For the continuing study, the bands ratio will be directly converted into the commonly used orientation function, $f_{c/z}$, by using the calibration equation of the figure 7 (b).

In situ results

Figure 8 (a) shows whole spectra recorded on non-deformed and large deformed (ε_{zz} = 1.6) samples during *in situ* experiments. Contrary to *post mortem* measurements, *in situ* spectra are noisy. This is caused by the important reduction in acquisition time to 5 s. Figure 8 (b) reports evolution of bands at 973 and 998 cm^{-1} (after spectral adjustment) in function of

various strain levels. Intensity of the 973 cm^{-1} band increases with the increasing strain. Just the opposite is noted for the 998 cm^{-1} one. This is in agreement with previous *post mortem* observations. At low strain, intensity variations are weak, become important at medium strain and become again weak at large strain. Moreover, we can note that these two bands also exhibit a peak shifting. Band at 973 cm^{-1} shifts towards low wavenumbers while the one at 998 cm^{-1} shifts towards the high wavenumbers. Raman shift is generally interpreted as an alteration of the atomic vibration (change in the inter-atomic distance) induced by mechanical stress applied at the chemical bond scale [24, 33, 34]. A shift towards low wavenumbers means that bonds are under an extension stress while a shift towards high wavenumbers is related to a compressive one. Thus, skeletal backbones C-C (band at 973 cm^{-1}) which are more and more oriented towards the stretching direction, experience a tensile stress. Reciprocally lateral alkyl groups CH_3 (band at 998 cm^{-1}) undergo a compressive stress.

Figure 9 shows both evolution of the orientation function $f_{c/z}$ (derived from Raman measurement by the calibration equation of the figure 7 (b)) and the true axial stress σ_{zz} in function of the true strain ε_{zz}. First remark is that *in situ* measurements allow collecting lot of spectra at different steps of the deformation leading to a more accurate description of the molecular orientation evolution. Secondly, evolution of the crystalline chains orientation can be described into three major domains with respect to the true strain. Its rigorous description has to take into account the high dependence of the initial radial orientation of macromolecules within spherulites (equatorial, diagonal and polar regions) with respect to the stress axis [35-38]. Figure 10 proposes a schematic model inspired on previous molecular models which illustrate the deformation micro-mechanisms occurring successively in crystalline lamellae of each region of spherulites.

i) In the elasto-viscoelastic regime, $\varepsilon_{zz} = 0 – 0.09$, $f_{c/z}$ is low and quite constant, $f_{c/z} = 0.05$. It indicates that crystalline chains are initially randomly oriented in the material.

Mechanisms of orientation are not yet active. At the early stages of stretching, it is just chains of the amorphous interlamellar layers which undergo deformation [39]. It involves disentanglement, extension and alignment of tie molecules between two adjacent crystalline lamellae. Deformation of amorphous phase is always at least partially reversible [40]. In equatorial regions of spherulites, lamellae are separated and they are subject to a bending solicitation as Nitta et al. proposed it [41]. Furthermore, the existence of a local compressive strain in polar regions induces a lamellar merger and also a lamellar bending. The deformation in diagonal regions is caused by amorphous chains extension and inter-lamellar shearing [42].

ii) In the plastic domain, ε_{zz} = 0.09 – 0.8, $f_{c/z}$ increases progressively from 0.05 to 0.48. This is related to the beginning of the crystalline chains orientation towards the tensile axis. At the yield point, amorphous phase cannot accommodate any more the deformation and this is crystals which are affected in turn. Blocks of crystals in equatorial position, attached by tie molecules in extension, are breaked up into smaller folded chains blocks [8-10]. Result is quite identical in polar regions where crystal blocks are at first pulled out of the lamellae and then rotate towards the tensile axis. In diagonal regions, the main effect of chain slip is to tilt macromolecules inside the crystalline lamellae and to align them more parallel to the stretching direction [43]. We can note that the inflection point of the increasing evolution of the orientation function is localized at ε_{zz} = 0.85, $f_{c/z}$ = 0.36. It suggests that the orientation mechanisms of crystalline chains take a predominant place for this particular strain level.

iii) In the last plastic-hardening domain, ε_{zz} = 0.8 – 1.6, the orientation function continues to increase but its progression becomes milder. Proportion of crystalline chains which experience tilt towards the tensile axis becomes lower, all being already oriented. Approaching the rupture deformation, orientation function is maximal and quite constant $f_{c/z}$ = 0.74. It suggests that crystalline chains have achieved their maximal orientation level before the material rupture. The initial lamellar structure is thus transformed into a micro-fibrillar

structure with both amorphous and crystalline chains oriented in the tensile direction [8-10]. Thus, the material exhibits an important macromolecular anisotropy [44].

Figure 11 compare evolutions of the orientation's function, $f_{c/z}$, determined in *post mortem* and *in situ* measurements in function of the true axial strain. We have to precise that the strains considered for *post mortem* results correspond to the residual true strain recorded after material recovering. For example an iPP deformed at $\varepsilon_{zz} = 1.2$ is characterized $f_{c/z} = 0.62$. After material recovering at $\varepsilon_{zz,r} = 0.79$, $f_{c/z}$ becomes lower, $f_{c/z} = 0.35$. The noted differences evidence a disorientation of the crystalline chains during the material recovering sequence noted $\Delta f_{c/z}$. This is consistent with the recovery phenomenon which occurs between the deformation stop and the *post mortem* microstructural analysis [16-18]. Indeed evolution of the deformed semi-crystalline microstructure is time-dependent and unstable. After unloading, the oriented crystal blocks tend to recover their initial random orientation due to the elastic response of the extended tie molecules in the amorphous interlamellae layers. The molecular model presented in figure 12 illustrates the strain recovering associated to the crystalline disorientation which occurs during the material recovery. Figure 13 presents the evolution of the crystalline disorientation $\Delta f_{c/z}$ with respect to the strain level ε_{zz} achieved in load for *post mortem* samples. Disorientation becomes more and more pronounced with the strain because the proportion of crystals blocks affected by the recovering mechanism is higher. This result evidences the main advantage of performing *in situ* experiments namely the measured orientation level corresponds exclusively to the uniaxial deformation, "parasite" contribution of the recovery being avoided.

CONCLUSION

Molecular orientation of the crystalline phase of isotactic polypropylene (iPP) was investigated by polarized Raman spectroscopy. In a fixed polarisation configuration, we have

established a measurement method based on the intensity sensitivity of specific Raman scattering bands at 973 and 998 cm^{-1} to molecular orientation. We proposed the ratio of their integrated intensity as an indicator of orientation. Firstly, the reliability of the method was validated by comparing Raman results with those found by Wide Angle X-ray Scattering on *post mortem* deformed samples (WAXS-Debye-Scherrer method). A good correlation was found. On the basis of this result, method is then applied to follow the crystalline phase orientation in real-time with the deformation. The experimental set-up developed for this purpose combines a VidéoTraction^{TM}-controlled tensile machine and a Raman spectrometer. It allows matching one true state of the deformation to one microstructural state with less than 5 s time resolution. Our results agree well with general descriptive model of semi-crystalline polymer deformation suggest by the past by Peterlin [8] and Schultz [9]. Results clearly evidence the recovery phenomenon occurring after sample unloading and confirm the use of in-real-time measurements.

Further works should be devoted to a closer examination of the amorphous phase evolution during deformation more precisely the macromolecular disentanglement and elongation during the elastic and visco-elastic regimes. Collection of data both on amorphous and crystalline phase would be give access to a more complete overview of the micro-structural mechanisms of deformation and a better understanding of the resistance properties of semi-crystalline polymers.

REFERENCES

Part1

1. I.M. Ward, *Mechanical Properties of Solid Polymers,* Wiley-Interscience, London (1971).

2. R.J. Samuels, In *Plastic Deformation of Polymers,* A. Peterlin, Marcel Dekker, New York (1971).

3. R.J. Samuels, *Structured Polymer Properties: The Identification, Interpretation, and Application of Crystalline Polymer Structure,* John Wiley & Sons, New York (1974).

4. A. Peterlin, *J. Mater. Sci.*, **6**, 490-508 (1971).

5. J. Schultz, *Polymer Materials Science,* Printice-Hall, Englewood Cliffs (1974).

6. K. Friedriech, In *Advances in Polymer Science, Crazing in Polymers 52/53*, H.H. Kausch, Springer-Verlag, Berlin-Heidelberg (1983).

7. J.M. Haudin, In *Plastic Deformation of Amorphous and Semi-Crystalline Materials*, B. Escaig and C. G'Sell, Les Editions de Physique, Les Ullis (1982).

8. C. G'Sell and A. Dahoun, *Mater. Sci. Eng*., **175**, 183-199 (1994).

9. D.L. Gerrard and W.F. Maddams, *Appl. Spec. Rev*., **22**, 251-334 (1986).

10. S.J. Spells, In *Characterization of Solid Polymers: New Techniques and Developments*, S.J. Spells, Chapman & Hall, London (1994).

11. G. Xue, *Prog. Polym. Sci.*, **19**, 317-388 (1994).

12. J.L. Koenig, *Spectroscopy of Polymers*, 2nd edition, Elsevier Science, New York (1999).

13. R.G. Snyder and J.H. Schachtshneider, *Spectrochim. Acta A*, **20**, 853-869 (1964).

14. H. Tadokoro, M. Kobayashi, M. Ukita, K. Yasufuku, S. Murahashi and T. Torii, *J. Chem. Phys.*, **42**(4), 1432-1448 (1965).

15. G. Zerbi and L. Piseri, *J. Chem. Phys*, **49**, 3840 (1964).

16. G.V. Fraser, P.J. Hendra, D.S. Watson, M.J. Gall, H.A. Willis and M.E.A. Cudby, *Spectrochim. Acta A*, **29**, 1525-1533 (1972).

17. J.M. Chalmers, H.G.M. Edwards, J.S. Lees, D.A. Long, M.W. Mackenzie and H.A. Willis, *J. Raman Spec.*, **22**(11), 613-618 (1991).

18. J. Martin, P. Bourson, A. Dahoun and J.M. Hiver, *Appl. Spec.*, **63** (12), 1377-1381 (2009).

19. D.I. Bower, *J. Polym. Sci.*, **10**, 2135-2153 (1972).

20. J. Purvis and D.I. Bower, *J. Polym. Sci.*, **14**,1461-1484 (1976).

21. L.D. Cambon, J.L. Ramonja and D.V. Luu, *J. Raman Spec*., **18**, 129-132 (1987).

22. M. Tanaka and R.J. Young, *J. Mater. Sci.*, **41**, 963-991 (2006).

23. P.H. Hermans and A. Weidinger, *J. Polym. Sci.*, **4**, 135-144 (1949).

24. B. Wunderlich, *Macromolecular Physics: Crystal structure, Morphology, Defects*, Academic Press, New York (1973).

25. B. Lotz and J.C. Wittman, *J. Polym. Sci*., **24**, 1541-1558 (1986).

26. C. G'Sell, J.M. Hiver and A. Dahoun, *Int. J. Solids Struc.*, **39**, 3857-3872 (2002).

27. F. Addiego, A. Dahoun, C. G'Sell and J.M. Hiver, *Polymer*, **47**(12), 4387-4399 (2006).

28. J.C. Viana, A.M. Cunha and N. Billon, *Polym. Eng. Sci.*, **39**(8), 1463-1472 (1999).

29. C. G'Sell and J.M. Hiver, French Patent #010542100, Bull Off INPI, 23 April: 2001.

30. C. G'Sell, J.M. Hiver, A. Dahoun and A. Souahi, *J. Mater. Sci.*, **27**, 5031-5039 (1992).

31. J. Martin, *Ph. D. Thesis*, Université Paul Verlaine, Metz, France (2009).

32. M. Ponçot, *Ph.D. Thesis*, Institut National Polytechnique de Lorraine, Nancy, France (2009).

33. K. Levenberg, *Quart. Appl. Math*., **2**, 164-168 (1944).

34. A. Marcellan, P. Colomban and A. Bunsell, *J. Raman Spec.*, **35**, 308-315 (2004).

35. R.A. Horsley and H.A. Nancarrow, *Brit. J. Appl. Phys*., **2**, 345-351 (1951).

36. E. Weynant, J.M. Haudin, C. G'Sell, *J. Mater. Sci.*, **15**, 2677-2692 (1980).

37. A. Dahoun, *Ph.D. Thesis*, Institut National Polytechnique de Lorraine, Nancy, France (1992).

38. R.A. Stein, *J. Polym. Sci*., **31**, 327-334 (1958).

39. Z.W. Wilchinsky, *Polymer*, **5**, 271-281 (1964).

40. G. Natta and P. Corradini, *Nuovo Cimento*, **1**, 40-51 (1960).

41. T.C. Damen, S.P.S. Porto and B. Tell, *Phys. Rev.*, **142**, 570 (1966).

Part2

1. J. Martin, M. Ponçot, P. Bourson, A. Dahoun and J.M. Hiver, *Polym. Eng. Sci.*, under submission (2009).

2. I.M. Ward, *Mechanical Properties of Solid Polymers*, Wiley-Interscience, London (1971).

3. R.J. Samuels, *Structured Polymer Properties: The Identification, Interpretation, and Application of Crystalline Polymer Structure*, John Wiley & Sons, New York (1974).

4. R.J. Young and P.A. Lovell, *Introduction to Polymers*, Chapman & Hall, New York (1981).

5. C. G'Sell, In *Plastic Deformation of Amorphous and Semi Crystalline Materials*, B. Escaig and C. G'Sell, Les Editions de Physique, Les Ullis (1982).

6. B. Wunderlich, *Macromolecular Physics: Crystal Structure, Morphology, Defects*, Academic Press, New York (1973)

7. U.W. Gedde, *Polymer Physics*, Kluwer Academic Publishers, Dordrecht (1995)

8. A. Peterlin, *J. Mater. Sci.*, **6**, 490-508 (1971).

9. J. Schultz, *Polymer Materials Science*, Printice-Hall, Englewood Cliffs (1974).

10. K. Friedriech, In *Advances in Polymer Science, Crazing in Polymers 52/53*, H.H. Kausch, Springer-Verlag, Berlin-Heidelberg (1983).

11. C. G'Sell and J.J. Jonas, *J. Mater. Sci.*, **14**, 583-591 (1979).

12. C. G'Sell, N.A. Aly-Hellah and J.J. Jonas, *J. Mater. Sci.*, **18**, 1731-1742 (1983).

13. C. G'Sell and J.M. Hiver, French Patent #010542100, Bull. Off. INPI, 23 April: 2001.

14. C. G'Sell, J.M. Hiver, A. Dahoun and A. Souahi, *J. Mater. Sci.*, **27**, 5031-5039 (1992).

15. C. G'Sell, J.M. Hiver and A. Dahoun, *Int. J. Solids Struc.*, **39**, 3857-3872 (2002).

16. R.H. Boyd, *Polymer*, **26**(3), 323-347 (1985).

17. L.R.G. Treloar, *The Physics of Rubber Elasticity*, Clarendon, Oxford (1975).

18. C. Jourdan, J.Y. Cavaille and J. Perez, *J. Polym. Sci.*, **27**, 2361-2384 (1989).

19. J. Martin, *Ph. D. Thesis*, Université Paul Verlaine Metz, France (2009).

20. M. Ponçot, *Ph. D., Thesis*, Institut National Polytechnique de Lorraine, Nancy, France (2009).

21. J. Martin, S. Margueron, M. Fontana, M. Cochez and P. Bourson, *Polym. Eng. Sci*., **50**(1), 138-143 (2009).

22. P. Colomban, J.M. Herrera Ramirez, R. Paquin, A. Marcellan and A. Bunsell, *Eng. Fract. Mechan.*, **73**, 2463-2475 (2006).

23. P. Colomban, *Compo. Sci. Tech.*, **69**, 1437-1441 (2009).

24. C. Galiotis, *Mater. Tech*., **8**, 203-209 (1993)

25. P.J. Hendra and W.F. Maddams, In *Polymer Spectroscopy*, John Wiley & Sons, A.H. Fawcett, Chichester (1996)

26. J.C. Rodriguez-Cabello, J.C. Merino and J.M. Pastor, *J. Raman Spec.*, **27**, 463-467 (1996).

27. R.J. Young and S.J. Eichorn, *Polymer*, **48**, 2-18 (2007).

28. K. Levenberg, *Quart. Appl. Math.*, **2**, 164-168 (1944).

29. T.C. Damen, S.P.S. Porto and B. Tell, *Phys. Rev.*, **142**(2), 570-574 (1966)

30. R.G. Snyder and J.H. Schachtschneider, *Spectrochim. Acta A*, **20**, 853-869 (1964)

31. H. Tadokoro, M. Kobayashi, M. Ukita, K. Yasufuku, S. Murahashi and T. Torii, *J. Chem. Phys.*, **42**(4), 1432-1448 (1965).

32. P.H. Hermans and A. Weidinger, *J. Polym. Sci*., **4**, 135-144 (1949).

33. R.J. Young, In *Characterization of Solid Polymers, New Techniques and Developments*, Chapman & Hall, S.J. Spells, London (1994).

34. G. Gouadec and P. Colomban, *Prog. Cryst. Growth*, **53**, 1-56 (2007).

35. P.H. Geil, *Polymer Single Crystals*, Interscience Publishers, New York (1963).

36. E. Weynant, J.M. Haudin and C. G'Sell, *J. Mater. Sci*., **15**, 2677-2692 (1980).

37. J.M. Haudin, In *Introduction à la Mécanique des Polymères*, Institut National Polytechnique de Lorraine, C. G'Sell and J.M. Haudin, Nancy (1995).

38. C. G'Sell and A. Dahoun, *Mater. Sci. Eng*., **175**(A), 183-199 (1994).

39. P.B. Bowden, R.J. Young, *J. Mater. Sci*., **9**, 2034-2051 (1974).

40. J.D. Ferry, *Viscoelastic Properties of Polymers*, Wiley, New York (1980).

41. K.H. Nitta and M. Takayanagi, *J. Polym. Sci*., **37**, 357-368 (1999).

42. L. Lin and A.S. Argon, *J. Mater. Sci*., **29**, 294-323 (1994).

43. Z. Bartczak, S.A. Argon and R.E. Cohen, *Macromol*., **25**(19), 5036-5053 (1992).

44. C. G'Sell, A Dahoun,V. Favier, J.M. Hiver, M.J. Philippe and G.R. Canova, *Polym. Eng. Sci*., **37**, 1702-1711, (1997).

Table 1: Preparation of *post mortem* iPP samples uniaxially stretched. ε_{zz} is the strain achieved in load just before unloading, $\varepsilon_{zz,r}$ is the residual strain measured 3 h after unloading.

$\boldsymbol{\varepsilon_{zz}}$	0.06	0.15	0.3	0.5	0.8	1	1.2
$\boldsymbol{\varepsilon_{zz,r}}$	0.008	0.04	0.15	0.31	0.52	0.65	0.79

FIGURES CAPTIONS

Figure 1: Geometry of the tensile test specimen machined out from an injection-molded plate.

Figure 2: Microstructure of injection-molded specimen within the depth. Optical microscopic view under polarized light performed on a microtomed cross-section.

Figure 3: General diagram of the VidéoTraction^{TM} system combined with a Raman spectrometer.

Figure 4: (a) Evolution of the tensile true stress-strain curve (σ_{zz} - ε_{zz}) of iPP recorded at 30 °C during monotonous loading at constant true strain 5.10^{-3} s^{-1}. (b) Example of the production of a stretched sample for *post mortem* analysis, deformed in load at 0.8 (step 0 to 1), unloaded at 0.7 (step 1 to 2) and recovered at 0.52 maintaining zero stress for 3 h (step 2 to 3).

Figure 5: Wide Angle X-ray Scattering (WAXS) patterns obtained on iPP samples uniaxially deformed, unloaded and then recovered at different residual true axial strains $\varepsilon_{zz,r}$: (a) 0.0, (b) 0.15, (c) 0.52 and (d) 0.79.

Figure 6: Influence of deformation on polarized Raman spectra of iPP (x(zz)x), (a) 750 – 1450 cm^{-1} and (b) 950 – 1015 cm^{-1}. Raman analyses are performed on *post mortem* deformed samples.

Figure 7: (a) Superposed evolutions of the orientation function $f_{c/z}$ and the bands ratio I_{973}/I_{998} in function of residual strain of iPP. (b) Linear regression between $f_{c/z}$ and I_{973}/I_{998}.

Figure 8: Influence of deformation on polarized Raman spectra of iPP (x(zz)x), (a) 750 – 1450 cm^{-1} and (b) 950 – 1015 cm^{-1}. Raman analyses are performed *in situ* with the deformation.

Figure 9: Evolution of the orientation function $f_{c/z}$ in function of strain of iPP. $f_{c/z}$ is calculated from Raman measurements performed *in situ* with the deformation.

Figure 10: Schematic illustration of the crystalline phase orientation occurring during the uniaxial deformation of the iPP microstructure. (inspired from Schultz [9] and Friedriech's models [10])

Figure 11: (a) Evolution of the orientation function $f_{c/z}$ in function of strain of iPP. Comparison between *post mortem* and *in situ* measurements. (b) Evolution of the crystalline phase disorientation $\Delta f_{c/z}$ in iPP relaxed material in function of various strain level achieved in load.

Figure 12: Schematic illustration of the crystalline phase disorientation occurring in iPP microstructure during relaxation sequence of a uniaxially stretched sample.

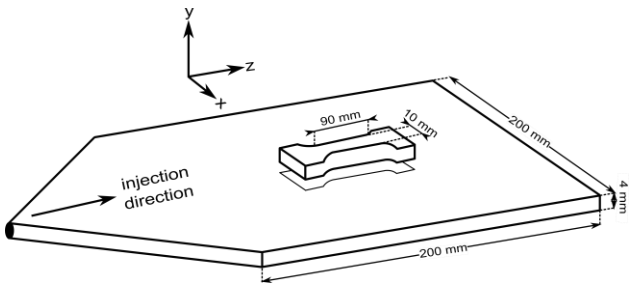

Figure 1: Geometry of the tensile test specimen machined out from an injection-molded plate.

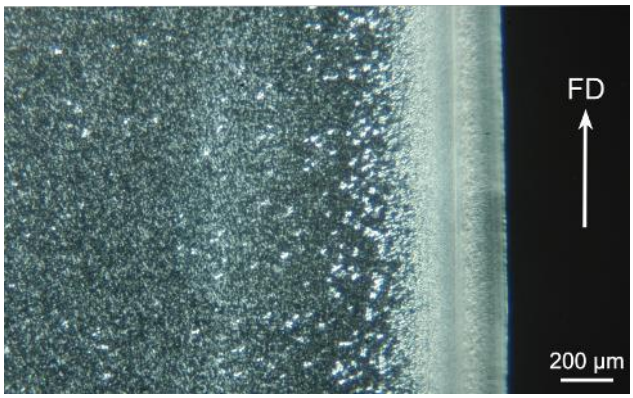

Figure 2: Microstructure of injection-molded specimen within the depth. Optical microscopic view under polarized light performed on a microtomed cross-section.

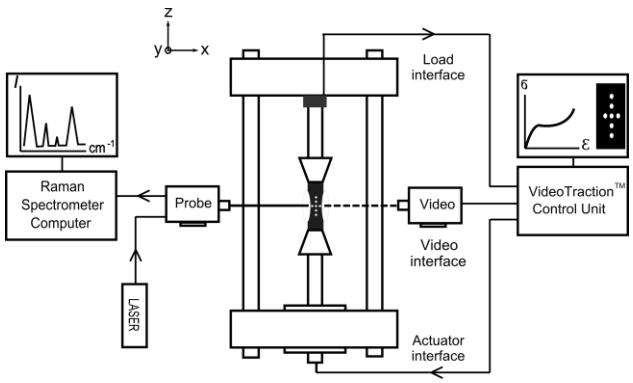

Figure 3: General diagram of the VidéoTraction^{TM} system combined with a Raman spectrometer.

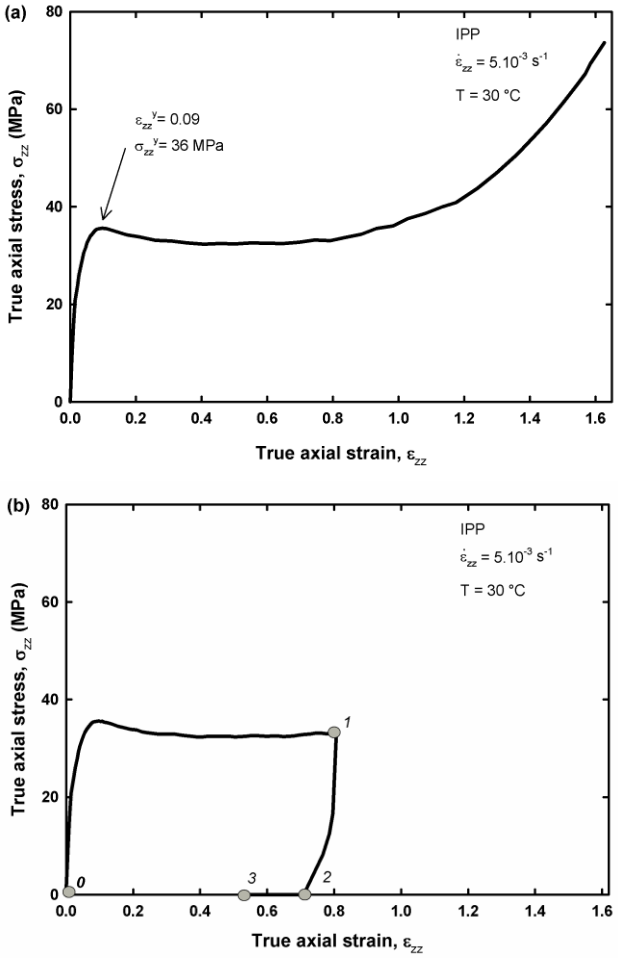

Figure 4: (a) Evolution of the tensile true stress-strain curve (σ_{zz} - ε_{zz}) of iPP recorded at 30 °C during monotonous loading at constant true strain 5.10^{-3} s^{-1}. (b) Example of the production of a stretched sample for *post mortem* analysis, deformed in load at 0.8 (step 0 to 1), unloaded at 0.7 (step 1 to 2) and recovered at 0.52 maintaining zero stress for 3 h (step 2 to 3).

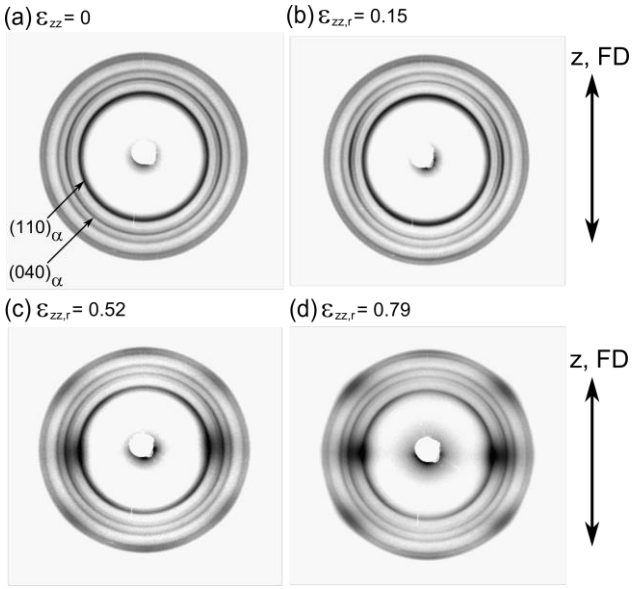

Figure 5: Wide Angle X-ray Scattering (WAXS) patterns obtained on iPP samples uniaxially deformed, unloaded and then recovered at different residual true axial strains $\varepsilon_{zz,r}$: (a) 0.0, (b) 0.15, (c) 0.52 and (d) 0.79.

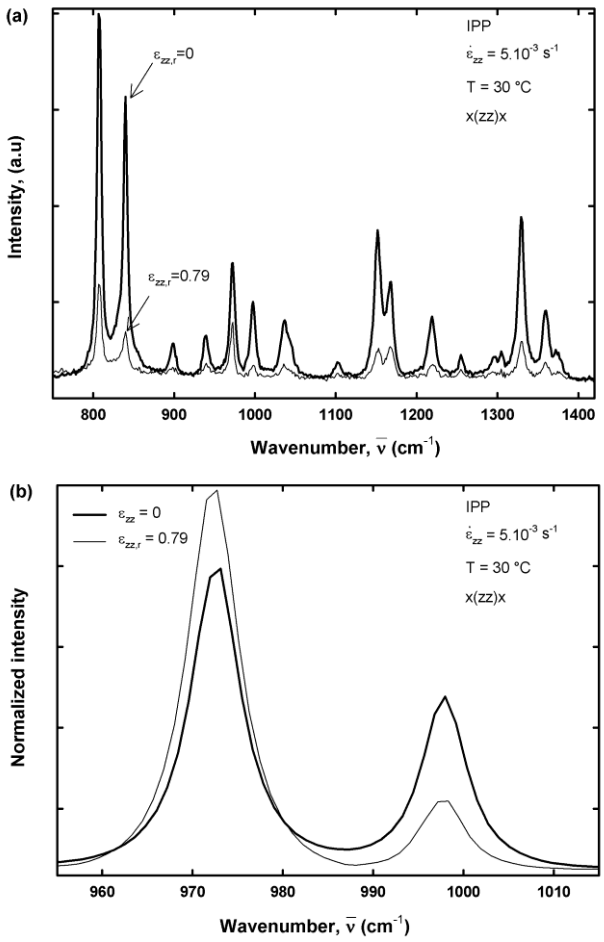

Figure 6: Influence of deformation on polarized Raman spectra of iPP (x(zz)x), (a) 750 – 1450 cm^{-1} and (b) 950 – 1015 cm^{-1}. Raman analyses are performed on *post mortem* deformed samples.

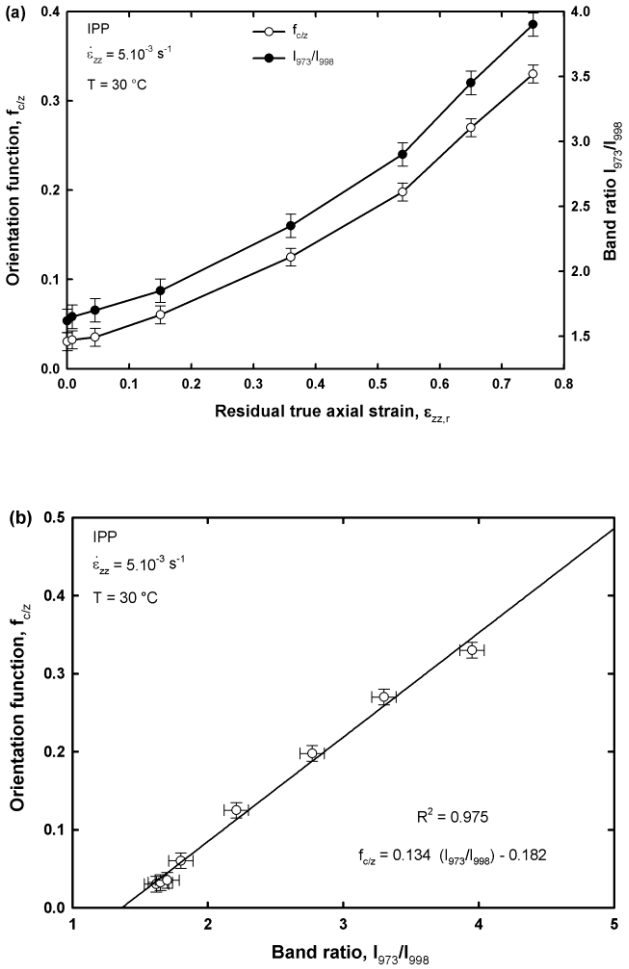

Figure 7: (a) Superposed evolutions of the orientation function $f_{c/z}$ and the bands ratio I_{973}/I_{998} in function of residual strain of iPP. (b) Linear regression between $f_{c/z}$ and I_{973}/I_{998}.

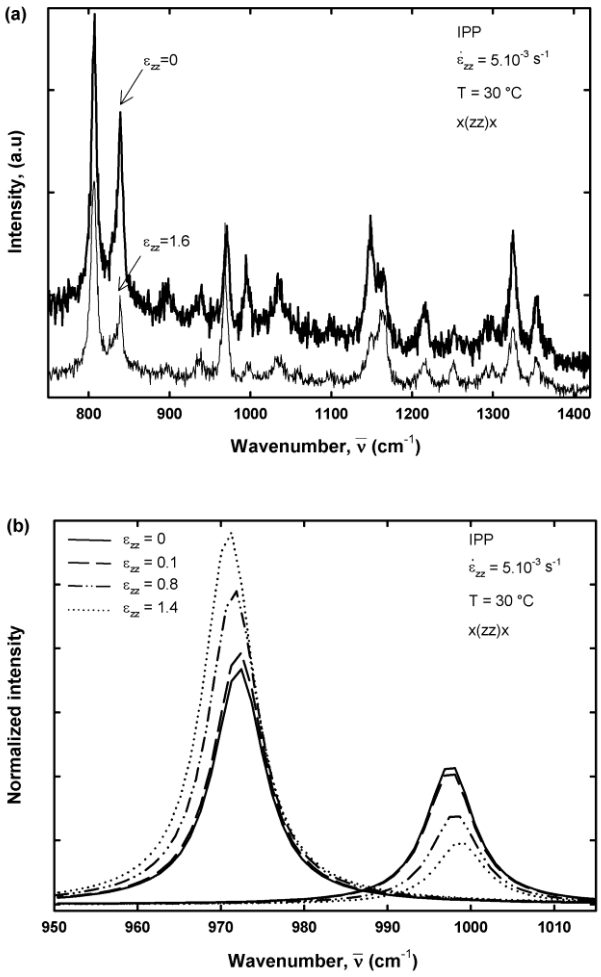

Figure 8: Influence of deformation on polarized Raman spectra of iPP (x(zz)x), (a) 750 – 1450 cm^{-1} and (b) 950 – 1015 cm^{-1}. Raman analyses are performed *in situ* with the deformation.

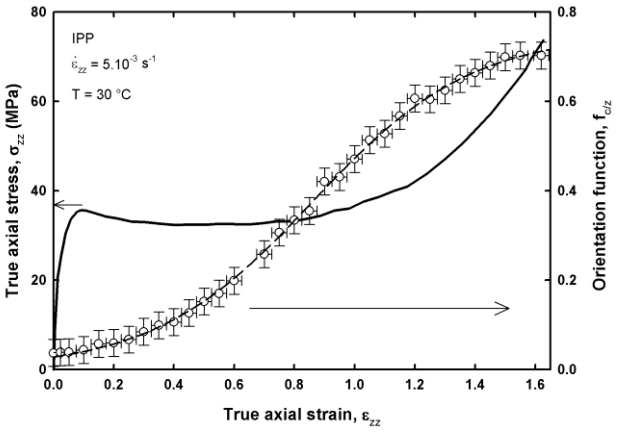

Figure 9: Evolution of the orientation function $f_{c/z}$ in function of strain of iPP. $f_{c/z}$ is calculated from Raman measurements performed *in situ* with the deformation.

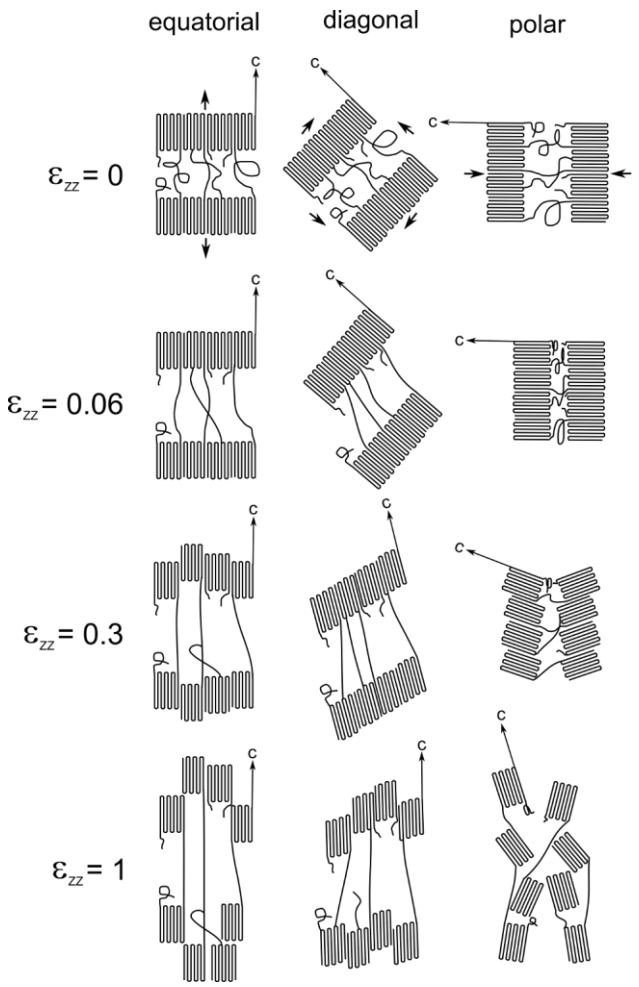

Figure 10: Schematic illustration of the crystalline phase orientation occurring during the uniaxial deformation of the iPP microstructure. (inspired from Schultz [9] and Friedriech's models [10])

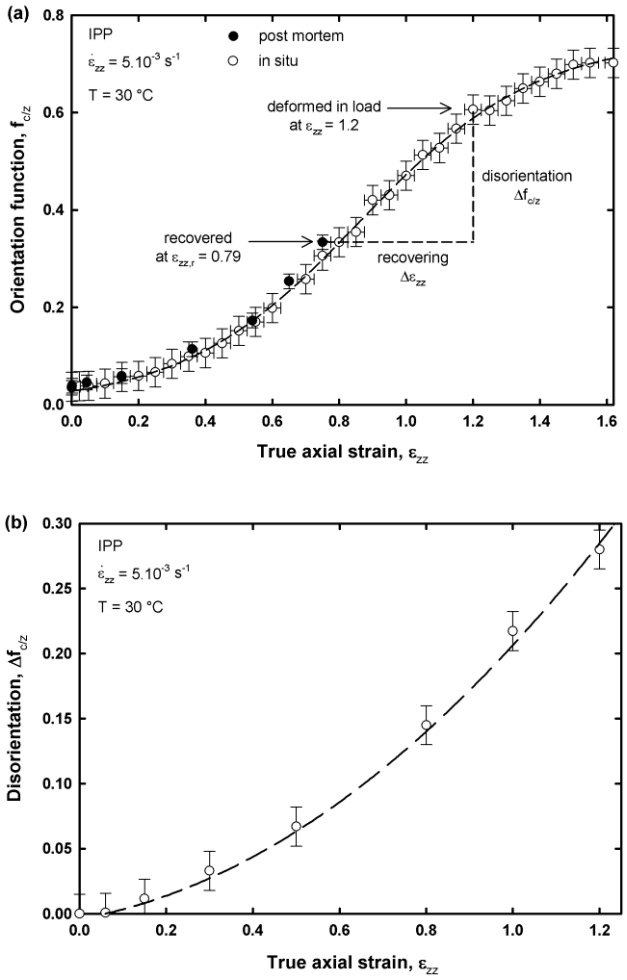

Figure 11: (a) Evolution of the orientation function $f_{c/z}$ in function of strain of iPP. Comparison between *post mortem* and *in situ* measurements. (b) Evolution of the crystalline phase disorientation $\Delta f_{c/z}$ in iPP relaxed material in function of various strain level achieved in load.

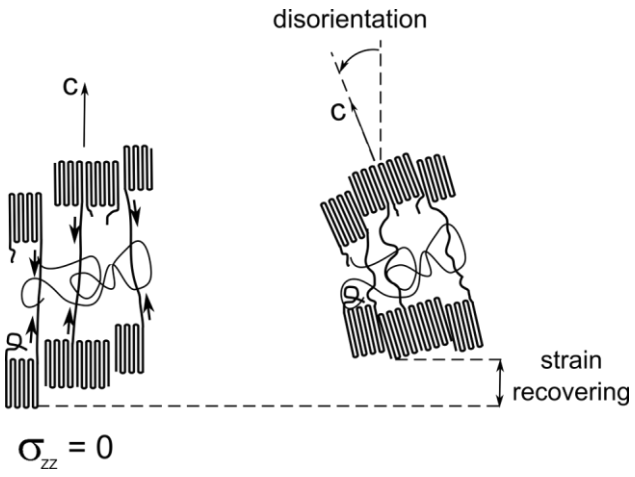

Figure 12: Schematic illustration of the crystalline phase disorientation occurring in iPP microstructure during relaxation sequence of a uniaxially stretched sample.